Letter

Second-order anomalous Hall effect controlled by electric fields in altermagnets

Arnob Mukherjee, Biplab Sanyal, Annica M. Black-Schaffer,* and Ankita Bhattacharya*,†
Department of Physics and Astronomy, Uppsala University, Box 516, S-75120 Uppsala, Sweden

(Received 27 October 2025; accepted 11 May 2026; published 3 June 2026)

Altermagnets are a recently discovered class of compensated magnets with momentum-dependent spin splittings and unusual transport properties, even without a net magnetization. In the presence of combined fourfold rotation and time-reversal ($C_4\mathcal{T}$) symmetry, linear and also second order, driven by a Berry curvature dipole, anomalous Hall responses are forbidden in any pure d-wave altermagnet. Nevertheless, here we find that the nontrivial quantum metric of the occupied Bloch states allows for an electric field induced Berry curvature dipole, which generates a strong and tunable second-order Hall current, enabling it to be switched on or off by simply adjusting the relative orientation between the symmetry-reducing dc field and the ac probe field. Specifically, we investigate the electric field induced second-order anomalous Hall response in a two-dimensional Rashba-coupled altermagnet with varying $d_{x^2-y^2}$ (B_{1g}) and d_{xy} (B_{2g}) altermagnet symmetry to capture all possibilities. Crucially, the nonlinear signal is highly sensitive to the underlying symmetry of the altermagnetic order at specific doping levels, offering a purely electrical method to distinguish distinct altermagnetic orders. Our results position altermagnets as a promising platform for controllable nonlinear transport and spintronic applications.

DOI: 10.1103/wb4y-tzln

Introduction. The discovery of altermagnets (AMs) has revealed a new class of magnetic order that bridges ferromagnets (FMs) and antiferromagnets (AFMs), exhibiting momentum-dependent spin splitting but zero net magnetization [1–7]. Unlike conventional (Néel) AFMs that preserve time-reversal symmetry ($\mathcal{T}$) through spin-compensated sublattices related by translation or inversion ($\mathcal{P}$), AM breaks global $\mathcal{T}$ while their sublattices are instead connected by crystalline point-group operations, such as rotations (C_n) or mirrors ($\mathcal{M}$) [7,8]. Consequently, AMs have been shown to host exotic electronic features, such as symmetry-protected nodal lines, Weyl planes [9], and momentum-locked spin textures [10], all while suppressing stray magnetic fields, thus making AMs promising candidates for advanced spintronic and topological devices [11,12].

In AMs, the Berry curvature (BC) exhibits quadrupolar or higher-order multipolar symmetry in momentum space, resulting in a vanishing momentum-space average and, consequently, the absence of any BC-driven linear anomalous Hall response [13,14], despite broken $\mathcal{T}$. Consequently, the leading anomalous Hall response may only emerge at second order. Recently, such second-order anomalous Hall effect (SAHE) has attracted considerable interest due to its fundamental connection to the quantum geometry of Bloch states and its potential for promising technological applications [15–22]. The primary driver for this SAHE is the dipole moment of the asymmetric distribution of the BC over the occupied state, namely, the Berry curvature dipole (BCD) [15,22]. In addition to requiring broken $\mathcal{P}$, SAHE is subject to strict crystallographic symmetry constraints [15]. In terms of d-wave AMs, both $\mathcal{T}$ and fourfold rotational (C_4) symmetries are broken individually, but the combined $C_4\mathcal{T}$ is preserved. As a consequence, recent works have shown that the second-order anomalous Hall response is forbidden in AMs and, subsequently, only nonlinear Hall responses at the third order have so far been thought to be possible [13,23–26].

Through a parallel development, recent theoretical [27] and experimental [28,29] works have demonstrated that the SAHE can also occur in systems where the inherent BCD is symmetry forbidden, if instead mediated by the Berry connection polarizability (BCP) or, equivalently, the band-normalized quantum metric (QM), i.e., the real part of the quantum geometric tensor. [18,30,31]. An external dc electric field can induce a finite field-induced BCD through the nontrivial QM of the occupied Bloch bands, making the SAHE present even in systems where the inherent BCD-induced SAHE is absent and, importantly, also provide greater external tunability. Notably, this electric field driven SAHE is distinct from the QM dipole induced intrinsic (independent of relaxation time) SAHE, reported in AMs [32] and $\mathcal{PT}$-symmetric AFM [18].

In this work, we establish a Hall response in AMs already at second order, driven, and thereby tunable, by a dc electric field. For a general treatment, we consider two-dimensional (2D) hybrid AMs. While prototypical AMs such as RuO_2 realize $d_{x^2-y^2}$ (B_{1g}) spin splitting within the tetragonal point group D_{4h} [33–35], theoretical classifications have

*These authors contributed equally to this work.
†Contact author: ankita.bhattacharya@physics.uu.se

Published by the American Physical Society under the terms of the Creative Commons Attribution 4.0 International license. Further distribution of this work must maintain attribution to the author(s) and the published article's title, journal citation, and DOI. Funded by Bibsam.

emphasized that both B_{1g} ($d_{x^2-y^2}$) and B_{2g} (d_{xy}) AM order parameters, belonging to different irreducible representations of D_{4h}, can coexist once the crystal symmetry is reduced [36,37]. In fact, mixing between different d-wave AM symmetries is known to occur through strain, easily achievable in thin films [38–41] or surface termination [37,42]. Experimental techniques such as nanoscale domain engineering [43,44] also allow for controlled tuning between these symmetry limits. Motivated by these developments, we consider a hybrid altermagnetic order, that continuously interpolates between the B_{1g} and B_{2g} irreducible representations, capturing at the same time both distinct and mixed d-wave symmetry states. We also consider AMs that inherently host Rashba spin-orbit coupling (RSOC) due to common structural asymmetry [24,45], which ensures the broken $\mathcal{P}$ required for any finite SAHE [15].

Using hybrid AMs with RSOC as a realistic platform for AMs, we theoretically establish the existence of an electric field induced BCD-assisted SAHE in AMs. In particular, this exploits the BCP or equivalently, the QM, to overcome the $C_4\mathcal{T}$ constraints that otherwise prevent an inherent BCD-induced SAHE. Remarkably, we also find that the electric field induced SAHE varies substantially in magnitude between the $d_{x^2-y^2}$ and d_{xy} limits in certain doping regimes, thus enabling a purely electrical route to distinguish the two altermagnetic orders. Our findings establish AMs as a powerful platform to realize highly tunable nonlinear Hall transport already at second order, driven by quantum geometric effects.

Model hybrid altermagnet (AM). To investigate the SAHE in hybrid AMs, we introduce a minimal two-band Hamiltonian defined on a 2D square lattice, which effectively encodes the AM properties at low energies. In this model, we phenomenologically mix the B_{1g} and B_{2g} components of the altermagnetic orderings to capture the essential physics of a hybrid AM. The tight-binding Hamiltonian is given by [46–48]

$$H(\mathbf{k}) = \epsilon(\mathbf{k})\,\sigma_0 + \mathbf{h}(\mathbf{k})\cdot\boldsymbol{\sigma}, \tag{1}$$

where σ_ν denote the Pauli matrices for $\nu = 1, 2, 3$ and the 2×2 identity matrix for $\nu = 0$ acting in the spin-sublattice subspace. The components of the Hamiltonian are

$$\epsilon(\mathbf{k}) = -2t\,(\cos k_x + \cos k_y) - \mu, \tag{2}$$

$$\mathbf{h}(\mathbf{k}) = \{-\lambda\,\sin k_y,\ \lambda\sin k_x,\ t_{\rm am}\,\alpha\,(\cos k_x - \cos k_y) + t_{\rm am}\,(1-\alpha)\,\sin k_x \sin k_y\}, \tag{3}$$

where t denotes the nearest-neighbor hopping amplitude, μ is the chemical potential, λ denotes the RSOC strength, and $t_{\rm am}$ is the strength of the altermagnetic spin splitting, which encodes the spin-sublattice coupling of AMs into a spin-dependent hopping. We parametrize the relative weight of the two altermagnetic orders by $0 \leqslant \alpha \leqslant 1$. In two dimensions, AMs inherently exhibit RSOC due to structural asymmetry [24,45]. The case $\alpha = 1$ corresponds to a pure $d_{x^2-y^2}$ AM order arising from nearest-neighbor spin-dependent hopping, while $\alpha = 0$ yields pure d_{xy} AM order governed by next nearest neighbor spin-dependent hopping. Note that we here use the word "pure" to refer to a single irreducible representation of the altermagnetic order, not to the absence of ferromagnetic component (which is also not present in our work). Intermediate values of α then describe a mixture or hybrid of pure AMs that allows for studying all possible mixed-symmetry states, achievable, for example, by strain [38–41] or surface effects [37,42] . Such mixing can also significantly enrich the spin splitting. We further note that in two dimensions, AMs inherently exhibit RSOC due to structural asymmetry [24,45].

The square lattice Hamiltonian in Eq. (1) may be relevant for tetragonal AMs such as RuO_2 [33–35] and MnTe [43,44,49], and is directly relevant to quasi-2D layered compounds like $Ca_3Ru_2O_7$ that host both altermagnetism and RSOC [38]. Additionally, it naturally accommodates the $d_{x^2-y^2}$ (B_{1g}) and d_{xy} (B_{2g}) [2,3] orders whose hybridization we study.

Second-order anomalous Hall effect (SAHE). Although the Hamiltonian in Eq. (1) breaks $\mathcal{T}$, it exhibits no anomalous Hall response at linear order in an applied ac electric field $\mathcal{E}^\omega$ with frequency ω, owing to the presence of combined $C_4\mathcal{T}$ symmetry. Consequently, the leading anomalous Hall transport may at most arise at second order in $\mathcal{E}^\omega$. Within semiclassical Boltzmann theory, the second-order anomalous Hall current can be expressed as $j_i^{\rm AH} = \chi_{ijk}^{\rm AH}\,\mathcal{E}_j^\omega\,\mathcal{E}_k^\omega$, with the second-order transverse conductivity tensor $\chi_{ijk}^{\rm AH}$ [15]

$$\chi_{ijk}^{\rm AH} = \epsilon_{ilk}\,\frac{e^3\tau}{2\hbar^2(1+i\omega\tau)}\sum_n \int \frac{d^d\mathbf{k}}{(2\pi)^d}\, f_0\left(\partial_{k_j}\Omega_l^n\right), \tag{4}$$

where ϵ_{ilk} is the Levi-Civita symbol and f_0 is the equilibrium Fermi-Dirac distribution function and Ω_l^n is the lth component of BC of the nth band. Here, τ is the relaxation time that makes the SAHE an extrinsic effect, albeit the BC is fully intrinsic. The integral is the first moment of the BC over the occupied states, known as the Berry curvature dipole (BCD) [15]:

$$D_{jl} = \sum_n \int \frac{d^d\mathbf{k}}{(2\pi)^d}\, f_0\left(\partial_{k_j}\Omega_l^n\right). \tag{5}$$

For the BCD, or equivalently $\chi_{ijk}^{\rm AH}$, to be nonzero, inversion symmetry $\mathcal{P}$ must be broken; otherwise, the momentum derivative $\partial_{k_j}\Omega_l^n(\mathbf{k})$ transforms as an odd function of momentum, causing its Brillouin zone integral to vanish. In Eq. (1), the Rashba term λ explicitly breaks $\mathcal{P}$. Additionally, the BCD obeys a severe symmetry constraint; namely, the presence of two or more mirror lines in a crystal forces the SAHE to still vanish, while a single mirror line forces it to be orthogonal to that mirror plane [15,50,51]. Thus mirror symmetries $\mathcal{M}_{x,y}$, when present, constrain BCD and, thus, the SAHE.

Pure $d_{x^2-y^2}$ altermagnetic order, i.e., when $\alpha = 1$ in Eq. (1), breaks both $\mathcal{M}_x$ and $\mathcal{M}_y$ mirror symmetries, while purely d_{xy}, i.e., $\alpha = 0$, preserves both $\mathcal{M}_{x,y}$. The presence of both $\mathcal{M}_{x,y}$ thus directly prohibits any BCD-induced SAHE for $\alpha = 0$. In contrast, the absence of both mirror planes for $\alpha = 1$, in principle, should allow SAHE. However, the presence of combined $C_4\mathcal{T}$ symmetry in AMs has been shown to completely forbid BCD-driven SAHE for any values of α, thus forcing the leading order Hall transport to be third order [13,14,52,53]. In this work we find an extrinsic second-order transverse Hall response in the presence of a dc electric field in AMs, due to the nontrivial QM of the Bloch states.

Electric field induced SAHE. In the presence of a symmetry-reducing dc electromagnetic field $\mathbf{E}^{\rm dc}$, the BC of the Bloch electrons is modified due to the positional shift of Bloch electrons arising from interband mixing [17]. This results in a field-induced Berry connection that is expressed as $\mathcal{A}^E = \overleftrightarrow{\mathbf{G}}\,\mathbf{E}^{\rm dc}$, where $\overleftrightarrow{\mathbf{G}}$ is a second-rank tensor, called the BCP. The component G^n_{ab} of the BCP tensor is defined as [17,54,55]

$$G^n_{ab}(\mathbf{k}) = 2\,\mathrm{Re}\sum_{m\neq n}\frac{\mathcal{A}^{nm}_a(\mathbf{k})\,\mathcal{A}^{mn}_b(\mathbf{k})}{\epsilon_n(\mathbf{k})-\epsilon_m(\mathbf{k})}. \tag{6}$$

Here, the interband Berry connection is $\mathcal{A}^{nm}_a(\mathbf{k}) = \langle u_n|i\partial_a|u_m\rangle$, where $\partial_a \equiv \partial_{k_a}$ and $|u_n\rangle$ is the periodic part of the nth unperturbed Bloch state, with ϵ_n the corresponding band energy. Notably, $G^n_{ab}(\mathbf{k})$ is closely linked with the QM, $g^n_{ab} = 2\sum_{m\neq n}\mathrm{Re}[\mathcal{A}^{nm}_a(\mathbf{k})\,\mathcal{A}^{mn}_b(\mathbf{k})]$, the real part of the quantum geometric tensor [30]. A nontrivial BCP, or equivalently QM, generates in turn a field-induced BC $\mathbf{\Omega}^E_n = \nabla_k \times \mathcal{A}^E_n$, which, similar to the original BC of the Bloch band, acts like a pseudomagnetic field in $\mathbf{k}$ space which yields a SAHE, just as the original BC in Eq. (4). The field-induced BC is especially important in those systems where either the intrinsic BC vanishes or the original BCD-induced SAHE is forbidden due to the symmetry constraints, as discussed above for AMs.

In typical Hall transport measurements, the applied electric field and the measured current are both restricted to the $x-y$ plane. Then, an external electric field applied at an angle θ relative to the x axis, such that $\mathbf{E}^{\rm dc} = E^{\rm dc}(\cos\theta, \sin\theta)$, induces a field-induced BC of the form [27,54,56]

$$\begin{aligned}\Omega^{\rm E}_{nz} = E^{\rm dc}\big[&\left(\partial_{k_x}G^n_{yx} - \partial_{k_y}G^n_{xx}\right)\cos\theta \\ &+ \left(\partial_{k_x}G^n_{yy} - \partial_{k_y}G^n_{xy}\right)\sin\theta\big],\end{aligned} \tag{7}$$

which is dependent on both the magnitude and direction of $\mathbf{E}^{\rm dc}$. This field-induced BC can lead to a finite field-induced BCD following Eq. (5) with an angular dependence $\mathbf{D}^{\rm E}(\theta) = (D^{\rm E}_{xz}(\theta), D^{\rm E}_{yz}(\theta))$. Due to the lowered symmetry in the presence of $\mathbf{E}^{\rm dc}$, a field-induced BCD then gives rise to the SAHE.

Finally, plugging the angular dependence of the BCD into Eq. (4), and recasting it through $\chi^{\rm AH} = j^{2\omega}/(E^\omega)^2$, we arrive at the second-harmonic current $j^{2\omega}$ [27,28],

$$j^{2\omega} = -\frac{e^3\tau}{2(1+i\omega\tau)\hbar^2}\,(\hat{z}\times\mathbf{E}^\omega)\,[\mathbf{D}^{\rm E}(\theta)\cdot\mathbf{E}^\omega], \tag{8}$$

where $\mathbf{E}^\omega$ is the in-plane ac Hall probe field that makes an angle ϕ with the x axis and satisfies the condition $E^\omega \ll E^{\rm dc}$. Here, we note that the probe field $\mathbf{E}^\omega$ is the same ac electric field as $\mathcal{E}^\omega$ introduced previously in the general analysis of the SAHE. Notably, the Hall response appears already at second order in the probe field $\mathbf{E}^\omega$, while the symmetry-breaking dc field $\mathbf{E}^{\rm dc}$ both enables it and offers additional tunability. As seen from Eq. (8), the maximum Hall response is obtained when $\mathbf{E}^\omega \parallel \mathbf{D}^{\rm E}(\theta)$, while it vanishes for $\mathbf{E}^\omega \perp \mathbf{D}^{\rm E}(\theta)$. Overall, the angular dependence $j^{2\omega}$ is intricate as it not only varies with θ through $\mathbf{D}^E(\theta)$ but also with ϕ, thus providing a high degree of external tunability of the SAHE. In two dimensions, only the two components χ_{yxx} and χ_{xyy} of the tensor $\chi^{\rm AH}_{ijk}$ are finite and independent. Thus $\chi^{\rm AH}$ simplifies to [18,27]

$$\chi^{\rm AH}(\theta,\phi) = \chi_{yxx}(\theta)\cos\phi - \chi_{xyy}(\theta)\sin\phi. \tag{9}$$

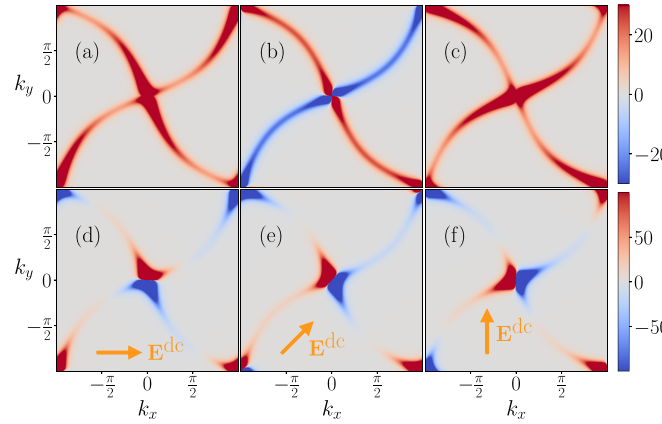


FIG. 1. Berry connection polarizability (BCP) tensor components for one of the bands: (a) G^1_{xx}, (b) G^1_{xy}, and (c) G^1_{yy} in the first Brillouin zone. Field-induced Berry curvature for the same band, $\Omega^{\rm E}(\mathbf{k})$, for dc-field orientations (d) $\theta = 0$, (e) $\pi/4$, and (f) $\pi/2$, with orange arrows indicating electric field directions. Calculations performed with $t = 1.0$, $t_{\rm am} = 0.5t$, $\alpha = 0.5$, $\mu = 0.3t$, and $\lambda = 0.08t$.

Our main results come from applying the above formalism to hybrid AMs, described by Eq. (1).

SAHE in altermagnets. We start by showcasing the $\mathbf{k}$-resolved distribution of the components of the BCP tensor or, equivalently, band-normalized QM for one of the two AM bands, setting $\alpha = 0.5$ in Figs. 1(a)–1(c).

For the other band, the contributions are exactly equal in magnitude but opposite in sign. For pure altermagnetic orders, i.e., for $\alpha = 0$ or $\alpha = 1$, the components of BCP tensors are shown in the Supplemental Material (SM) [57]. The corresponding band structures for these three α values are shown in the SM [57]. Consistent with expectations, the BCP values exhibit maxima at the band-touching points, due to the denominator in Eq. (6). The presence of a finite BCP leads to a finite BC, in accordance with Eq. (7), when an external dc electric field $\mathbf{E}^{\rm dc}$ is applied. For $\mathbf{E}^{\rm dc}$ oriented along the x ($\theta = 0$), $x = y$ ($\theta = \pi/4$), and $y(\theta = \pi/2)$, the field-induced BC Ω^E are shown in Figs. 1(d)–1(f), respectively. The $\mathbf{k}$-resolved distribution of Ω^E shows a clear dipolar structure. Not only the magnitude, but also the direction of the Ω^E and, thus, also the resulting BCD, can be externally tuned by changing the direction of $\mathbf{E}^{\rm dc}$ [27].

Once a finite and field-tunable BCD is confirmed, it is straightforward to express $\chi^{\rm AH}$ in terms of D_{xz} and D_{yz} following Eqs. (4) and (5). Figure 2 shows the momentum-resolved components of the Fermi-weighted Berry curvature dipole, i.e., the integrand of Eq. (5) for both bands again for $\alpha = 0.5$, with $\mathbf{E}^{\rm dc}$ oriented along the $x = y$ direction. These are then integrated over the Brillouin zone and summed over bands to yield the finite field-induced BCD. Finally, following Eq. (4), with its angular dependence in Eq. (9), we find an overall nonzero second-order Hall response. The complex angular variation of the resulting second-order Hall conductivity $\chi^{\rm AH}(\theta,\phi)$ in a hybrid AM is depicted in Fig. 3. It offers significant experimental control over the second-order Hall

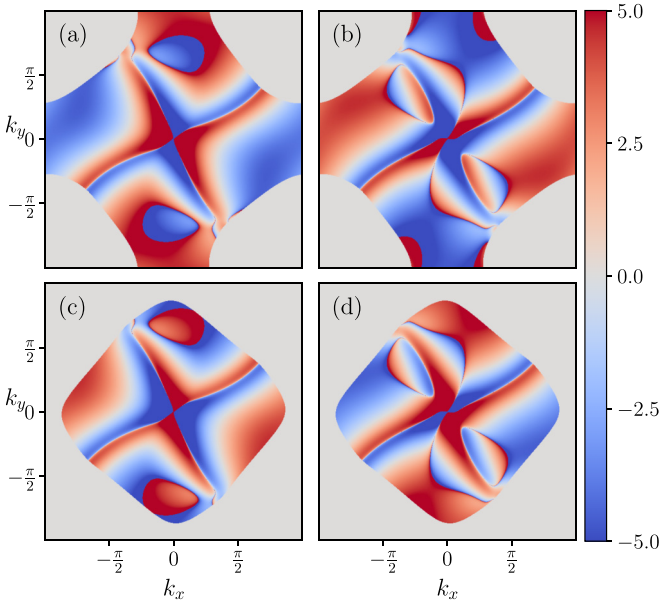


FIG. 2. Momentum distribution of the Fermi function weighted derivatives of the field-induced Berry curvature in signed logarithmic scale, $\mathrm{sign}(x)\ln(|x|+\varepsilon)$ for the two bands, (a) $f_0\ \partial_{k_x}\Omega_1^{\mathrm{E}}$, (b) $f_0\ \partial_{k_y}\Omega_1^{\mathrm{E}}$, and for band 2, (c) $f_0\ \partial_{k_x}\Omega_2^{\mathrm{E}}$, (d) $f_0\ \partial_{k_y}\Omega_2^{\mathrm{E}}$, evaluated at $\theta=\pi/4$. Parameters are the same as in Fig. 1.

current, enabling it to be switched on or off simply by adjusting the relative orientation of $\mathbf{E}^{\mathrm{dc}}$ and $\mathbf{E}^{\omega}$. These behaviors are similarly observed for the pure altermagnetic order, i.e., for $\alpha=1$ and $\alpha=0$; see the SM [57].

Remarkably, we find that the electric field induced SAHE exhibits a strong sensitivity in magnitude between different altermagnetic orders, at least for a range of doping levels, set by μ. The response is maximized at $\alpha=0$, corresponding to a pure d_{xy}-type altermagnetic order when $\mathbf{E}^{\mathrm{dc}}\perp\mathbf{E}^{\omega}$, but as α increases, the response χ^{AH} decreases and becomes negligible for $\alpha\to 1$, i.e., pure $d_{x^2-y^2}$ order; see Fig. 4(a). In contrast, when $\mathbf{E}^{\mathrm{dc}}\parallel\mathbf{E}^{\omega}$, χ^{AH} is found to be vanishingly small for both $\alpha=0$ and $\alpha=1$ as shown in Fig. 4(b). Thus, simply tuning the direction of either $\mathbf{E}^{\mathrm{dc}}$ or $\mathbf{E}^{\omega}$ provides a straightforward

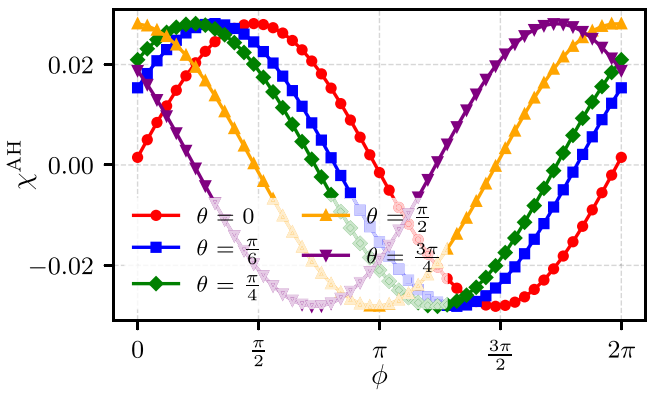


FIG. 3. Second-order Hall conductivity χ^{AH} as a function of angle ϕ, set by the ac driving field $\mathbf{E}^{\omega}$, for several different angles θ, set by the symmetry-breaking static field $\mathbf{E}^{\mathrm{dc}}$, with the x axis. χ^{AH} is scaled by the prefactor $\mathcal{A}=\frac{e^3\tau}{2(1+i\omega\tau)\hbar^2}$ and the parameters are the same as in Fig. 1.

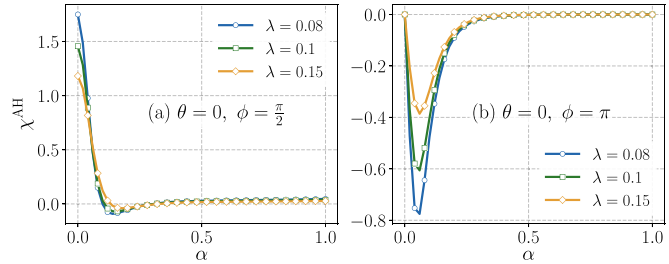


FIG. 4. Second-order Hall conductivity χ^{AH} as a function of α for different RSOC λ values and field orientations: (a) $\theta=0$, $\phi=\pi/2$ and (b) $\theta=0$, $\phi=\pi$ with $t=1$, $t_{\mathrm{am}}=0.5t$, and $\mu=0.3t$ (same as Fig. 1).

way to conclusively distinguish between pure orders d_{xy} and $d_{x^2-y^2}$. For the parameter choices used in the presented results, this doping range is found to be $-t<\mu<t$. We have also tested our results for smaller and larger t_{am}, which shifts the corresponding doping range, although it is still clearly present. In this doping regime, the system exhibits two holelike Fermi pockets for $\alpha=0$, whereas for $\alpha=0.5$ and $\alpha=1$, it features one electron and one hole Fermi pocket; see the SM [57]. When the Fermi surfaces (FSs) have the opposite curvature, their contributions to Hall transport tend to cancel each other, resulting in a nearly vanishing response. In contrast, when both FSs have the same curvature, their contributions add constructively, leading to a finite overall response. For example, in the doping regime with two electron pockets (regardless of α), the field-induced SAHE remains nonzero for both pure and hybrid altermagnetic symmetries; see the SM [57]. In this scenario, pure altermagnetic orders cannot be distinguished based on the second-order response, as all yield a finite signal.

These findings unambiguously establish the presence of a nonlinear Hall response in AM at second order and also offer an all-electrical approach to resolve pure altermagnetic orderings. As shown in Fig. 4, the electric field induced SAHE increases when the strength of RSOC λ decreases. Still, we recall that no SAHE is possible for $\lambda=0$ due to preserved $\mathcal{P}$. At first glance, this may seem nonintuitive. However, we note that for finite λ, RSOC opens gaps at the band-touching points in altermagnetic metals. When λ is small, these gaps are narrow, leading to an enhanced BCP [see Eq. (6)], which in turn amplifies the field-induced SAHE. The evolution of the two spin-split FSs with λ in various doping limits is shown in the SM [57].

Concluding remarks. In summary, we demonstrate that Rashba-coupled hybrid AMs provide a viable platform for electric field induced SAHE that arises due to the nontrivial QM of the Bloch bands. Although combined $C_4\mathcal{T}$ symmetry forbids both the linear anomalous Hall effect and the usual BCD-driven second-order Hall signal, we find that an external dc field lowers the symmetry and generates a finite field-induced BCD via the nontrivial QM of the occupied Bloch states, thereby generating a second-order Hall effect. Moreover, the intricate angular variation of the resulting second-order Hall conductivity $\chi^{\mathrm{AH}}(\theta,\phi)$ provides substantial experimental control over the second-order Hall current, allowing it to be toggled on or off by merely adjusting the relative orientation between the external dc field $\mathbf{E}^{\mathrm{dc}}$ and ac

probe field $\mathbf{E}^{\omega}$. Knowing the underlying Fermi surface, the SAHE can even probe the underlying altermagnetic form factor, peaking in the d_{xy} (B_{2g}) limit and decreasing toward $d_{x^2-y^2}$ (B_{1g}) configuration for $\mathbf{E}^{\mathrm{dc}} \perp \mathbf{E}^{\omega}$, which then provides a purely electrical means to distinguish the two.

These predictions are directly testable in candidate material platforms such as epitaxial RuO_2 [33–35], where strain or surface termination can realize hybrid B_{1g}–B_{2g} textures and provide the required inversion-symmetry breaking at interfaces that generate interfacial RSOC. To observe the SAHE, an experimental setup similar to the one used in Refs. [28,29] could be employed. Although intrinsic, i.e., τ-independent Berry connection polarizability dipole-induced SAHE can in principle arise in our TRS-broken system, it is always distinguishable from the extrinsic contribution reported here due to their distinct scaling behavior with τ; importantly, unlike the intrinsic contribution, the extrinsic SAHE is highly tunable by external means. More broadly, our results demonstrate that quantum geometry can enable nonlinear responses in systems where symmetry otherwise suppresses intrinsic BC effects, enabling functionalities such as on-chip frequency doubling and rectification in zero-moment magnets.

Acknowledgments. A.B and A.M.B.-S. acknowledge financial support from the Swedish Research Council (Vetenskapsrådet) Grant No. 2022-03963 and the European Union through the European Research Council (ERC) under the European Union's Horizon 2020 research and innovation programme (ERC-2022-CoG, Grant Agreement No. 101087096). Views and opinions expressed are, however, those of the author(s) only and do not necessarily reflect those of the European Union or the European Research Council Executive Agency. Neither the European Union nor the granting authority can be held responsible for them. B.S. acknowledges financial support from the Swedish Research Council (Grant No. 2022-04309), STINT Mobility Grant for Internationalization (Grant No. MG2022-9386) and DST-SPARC, India (Reference No. SPARC/2019-2020/P1879/SL). A.M. acknowledges the computational resources provided by the National Academic Infrastructure for Supercomputing in Sweden (NAISS) at NSC and PDC (Grant No. NAISS 2024/3-40) partially funded by the Swedish Research Council through Grant Agreement No. 2022-06725 and at UPPMAX (Grant No. NAISS 2025/2-203). B.S. also acknowledges the allocation of supercomputing hours granted by the EuroHPC JU Development Access call in LUMI-C supercomputer (Grant No. EHPC-DEV-2024D04-071) in Finland.

Data availability. The data that support the findings of this article are openly available [58].

[1] J. Krempasky, L. Šmejkal, S. D'souza, M. Hajlaoui, G. Springholz, K. Uhlířová, F. Alarab, P. Constantinou, V. Strocov, D. Usanov, *et al.*, Altermagnetic lifting of kramers spin degeneracy, Nature (London) **626**, 517 (2024).

[2] L. Šmejkal, J. Sinova, and T. Jungwirth, Emerging research landscape of altermagnetism, Phys. Rev. X **12**, 040501 (2022).

[3] L. Šmejkal, J. Sinova, and T. Jungwirth, Beyond conventional ferromagnetism and antiferromagnetism: A phase with nonrelativistic spin and crystal rotation symmetry, Phys. Rev. X **12**, 031042 (2022).

[4] R. Tamang, S. Gurung, D. P. Rai, S. Brahimi, and S. Lounis, Newly discovered magnetic phase: A brief review on altermagnets, arXiv:2412.05377.

[5] C. Song, H. Bai, Z. Zhou, L. Han, H. Reichlova, J. H. Dil, J. Liu, X. Chen, and F. Pan, Altermagnets as a new class of functional materials, Nat. Rev. Mater. **10**, 473 (2025).

[6] O. Gomonay, V. Kravchuk, R. Jaeschke-Ubiergo, K. Yershov, T. Jungwirth, L. Šmejkal, J. v. d. Brink, and J. Sinova, Structure, control, and dynamics of altermagnetic textures, npj Spintron. **2**, 35 (2024).

[7] P. A. McClarty and J. G. Rau, Landau theory of altermagnetism, Phys. Rev. Lett. **132**, 176702 (2024).

[8] Y. Yu, H. G. Suh, M. Roig, and D. F. Agterberg, Altermagnetism from coincident Van Hove singularities: application to κ-Cl, Nat. Commun. **16**, 2950 (2025).

[9] T. Jungwirth, R. M. Fernandes, J. Sinova, and L. Smejkal, Altermagnets and beyond: Nodal magnetically-ordered phases, arXiv:2409.10034.

[10] M. Naka, Y. Motome, and H. Seo, Altermagnetic perovskites, npj Spintron. **3**, 1 (2025).

[11] A. Bose, S. Vadnais, and A. Paramekanti, Altermagnetism and superconductivity in a multiorbital $t-j$ model, Phys. Rev. B **110**, 205120 (2024).

[12] T. Jungwirth, J. Sinova, P. Wadley, D. Kriegner, H. Reichlova, F. Krizek, H. Ohno, and L. Smejkal, Altermagnetic spintronics, arXiv:2508.09748.

[13] Y. Fang, J. Cano, and S. A. A. Ghorashi, Quantum geometry induced nonlinear transport in altermagnets, Phys. Rev. Lett. **133**, 106701 (2024).

[14] K. Takahashi, C. R. W. Steward, M. Ogata, R. M. Fernandes, and J. Schmalian, Elasto-Hall conductivity and the anomalous Hall effect in altermagnets, Phys. Rev. B **111**, 184408 (2025).

[15] I. Sodemann and L. Fu, Quantum nonlinear Hall effect induced by Berry curvature dipole in time-reversal invariant materials, Phys. Rev. Lett. **115**, 216806 (2015).

[16] Q. Ma, S.-Y. Xu, H. Shen, D. MacNeill, V. Fatemi, T.-R. Chang, A. M. Mier Valdivia, S. Wu, Z. Du, C.-H. Hsu, *et al.*, Observation of the nonlinear Hall effect under time-reversal-symmetric conditions, Nature (London) **565**, 337 (2019).

[17] Y. Gao, S. A. Yang, and Q. Niu, Field induced positional shift of Bloch electrons and its dynamical implications, Phys. Rev. Lett. **112**, 166601 (2014).

[18] H. Liu, J. Zhao, Y.-X. Huang, W. Wu, X.-L. Sheng, C. Xiao, and S. A. Yang, Intrinsic second-order anomalous Hall effect and its application in compensated antiferromagnets, Phys. Rev. Lett. **127**, 277202 (2021).

[19] C. Wang, Y. Gao, and D. Xiao, Intrinsic nonlinear Hall effect in antiferromagnetic tetragonal CuMnAs, Phys. Rev. Lett. **127**, 277201 (2021).

[20] A. Gao, Y.-F. Liu, J.-X. Qiu, B. Ghosh, T. V. Trevisan, Y. Onishi, C. Hu, T. Qian, H.-J. Tien, S.-W. Chen, *et al.*, Quantum

metric nonlinear Hall effect in a topological antiferromagnetic heterostructure, Science **381**, 181 (2023).
[21] N. Wang, D. Kaplan, Z. Zhang, T. Holder, N. Cao, A. Wang, X. Zhou, F. Zhou, Z. Jiang, C. Zhang, *et al.*, Quantum-metric-induced nonlinear transport in a topological antiferromagnet, Nature (London) **621**, 487 (2023).
[22] D. Kaplan, T. Holder, and B. Yan, Unification of nonlinear anomalous Hall effect and nonreciprocal magnetoresistance in metals by the quantum geometry, Phys. Rev. Lett. **132**, 026301 (2024).
[23] D. S. Antonenko, R. M. Fernandes, and J. W. F. Venderbos, Mirror Chern bands and Weyl nodal loops in altermagnets, Phys. Rev. Lett. **134**, 096703 (2025).
[24] P. Rao, A. Mook, and J. Knolle, Tunable band topology and optical conductivity in altermagnets, Phys. Rev. B **110**, 024425 (2024).
[25] S. Sorn and A. S. Patri, Signatures of hidden octupolar order from nonlinear Hall effects, Phys. Rev. B **110**, 125127 (2024).
[26] T. Farajollahpour, R. Ganesh, and K. Samokhin, Light-induced charge and spin Hall currents in materials with C_4K symmetry, npj Quantum Mater. **10**, 29 (2025).
[27] A. Bhattacharya and A. M. Black-Schaffer, Electric field induced second-order anomalous Hall transport in unconventional Rashba systems, Phys. Rev. B **111**, L041202 (2025).
[28] X.-G. Ye, H. Liu, P.-F. Zhu, W.-Z. Xu, S. A. Yang, N. Shang, K. Liu, and Z.-M. Liao, Control over Berry curvature dipole with electric field in WTe_2, Phys. Rev. Lett. **130**, 016301 (2023).
[29] J. Yang, L. Wei, Y. Li, L. Chen, W. Niu, J. Chen, J. Du, and Y. Pu, Electric field control of third-order nonlinear Hall effect, arXiv:2506.10657.
[30] P. Törmä, Essay: Where can quantum geometry lead us? Phys. Rev. Lett. **131**, 240001 (2023).
[31] G. Sala, M. T. Mercaldo, K. Domi, S. Gariglio, M. Cuoco, C. Ortix, and A. D. Caviglia, The quantum metric of electrons with spin-momentum locking, Science **389**, 822 (2025).
[32] M. Ezawa, Intrinsic nonlinear conductivity induced by quantum geometry in altermagnets and measurement of the in-plane Néel vector, Phys. Rev. B **110**, L241405 (2024).
[33] O. Fedchenko, J. Minár, A. Akashdeep, S. W. D'Souza, D. Vasilyev, O. Tkach, L. Odenbreit, Q. Nguyen, D. Kutnyakhov, N. Wind, *et al.*, Observation of time-reversal symmetry breaking in the band structure of altermagnetic RuO_2, Sci. Adv. **10**, eadj4883 (2024).
[34] D. T. Plouff, L. Scheuer, S. Shrestha, W. Wu, N. J. Parvez, S. Bhatt, X. Wang, L. Gundlach, M. B. Jungfleisch, and J. Q. Xiao, Revisiting altermagnetism in RuO_2: A study of laser-pulse induced charge dynamics by time-domain terahertz spectroscopy, npj Spintron. **3**, 17 (2025).
[35] Y. Guo, J. Zhang, Z. Zhu, Y.-y. Jiang, L. Jiang, C. Wu, J. Dong, X. Xu, W. He, B. He, *et al.*, Direct and inverse spin splitting effects in altermagnetic RuO_2, Adv. Sci. **11**, 2400967 (2024).
[36] R. M. Fernandes, V. S. de Carvalho, T. Birol, and R. G. Pereira, Topological transition from nodal to nodeless Zeeman splitting in altermagnets, Phys. Rev. B **109**, 024404 (2024).
[37] A. Ramires, From pure to mixed: Altermagnets as intrinsic symmetry-breaking indicators, arXiv:2502.19162.
[38] A. León, C. Autieri, T. Brumme, and J. W. González, Hybrid d/p-wave altermagnetism in $Ca_3Ru_2O_7$ and strain-controlled spin splitting, npj Quantum Mater. **10**, 98 (2025).
[39] B. Karetta, X. H. Verbeek, R. Jaeschke-Ubiergo, L. Šmejkal, and J. Sinova, Strain-controlled g- to d-wave transition in altermagnetic CrSb, Phys. Rev. B **112**, 094454 (2025).
[40] M. Khodas, S. Mu, I. Mazin, and K. Belashchenko, Tuning of altermagnetism by strain, Phys. Rev. B **113**, 104422 (2026).
[41] S. Li, Y. Zhang, A. Bahri, X. Zhang, and C. Jia, Altermagnetism and strain induced altermagnetic transition in Cairo pentagonal monolayer, npj Quantum Mater. **10**, 83 (2025).
[42] R. Tamang, S. Gurung, D. P. Rai, S. Brahimi, and S. Lounis, Altermagnetism and altermagnets: A brief review, Magnetism **5**, 17 (2025).
[43] O. Amin, A. Dal Din, E. Golias, Y. Niu, A. Zakharov, S. Fromage, C. Fields, S. Heywood, R. Cousins, F. Maccherozzi, *et al.*, Nanoscale imaging and control of altermagnetism in MnTe, Nature (London) **636**, 348 (2024).
[44] A. Hariki, A. Dal Din, O. J. Amin, T. Yamaguchi, A. Badura, D. Kriegner, K. W. Edmonds, R. P. Campion, P. Wadley, D. Backes, L. S. I. Veiga, S. S. Dhesi, G. Springholz, L. Šmejkal, K. Výborný, T. Jungwirth, and J. Kuneš, X-ray magnetic circular dichroism in altermagnetic α-MnTe, Phys. Rev. Lett. **132**, 176701 (2024).
[45] M. Amundsen, A. Brataas, and J. Linder, RKKY interaction in Rashba altermagnets, Phys. Rev. B **110**, 054427 (2024).
[46] T. Farajollahpour, R. Ganesh, and K. Samokhin, Berry curvature-induced transport signature for altermagnetic order, npj Quantum Mater. **10**, 77 (2025).
[47] B. Lu, K. Maeda, H. Ito, K. Yada, and Y. Tanaka, φ Josephson junction induced by altermagnetism, Phys. Rev. Lett. **133**, 226002 (2024).
[48] S. A. A. Ghorashi, T. L. Hughes, and J. Cano, Altermagnetic routes to Majorana modes in zero net magnetization, Phys. Rev. Lett. **133**, 106601 (2024).
[49] R. Yamamoto, L. A. Turnbull, M. Schmidt, J. C. Corsaletti Filho, H. J. Binger, M. Di Pietro Martínez, M. Weigand, S. Finizio, Y. Prots, G. M. Ferguson, U. Vool, S. Wintz, and C. Donnelly, Altermagnetic nanotextures revealed in bulk MnTe, Phys. Rev. Appl. **24**, 034037 (2025).
[50] C. Ortix, Nonlinear Hall effect with time-reversal symmetry: Theory and material realizations, Adv. Quantum Technol. **4**, 2100056 (2021).
[51] S. Nandy and I. Sodemann, Symmetry and quantum kinetics of the nonlinear Hall effect, Phys. Rev. B **100**, 195117 (2019).
[52] S. Sankar, R. Liu, C.-P. Zhang, Q.-F. Li, C. Chen, X.-J. Gao, J. Zheng, Y.-H. Lin, K. Qian, R.-P. Yu, X. Zhang, Z. Y. Meng, K. T. Law, Q. Shao, and B. Jäck, Experimental evidence for a Berry curvature quadrupole in an antiferromagnet, Phys. Rev. X **14**, 021046 (2024).
[53] L. Xiang, C. Zhang, L. Wang, and J. Wang, Third-order intrinsic anomalous Hall effect with generalized semiclassical theory, Phys. Rev. B **107**, 075411 (2023).
[54] S. Lai, H. Liu, Z. Zhang, J. Zhao, X. Feng, N. Wang, C. Tang, Y. Liu, K. Novoselov, S. A. Yang, *et al.*, Third-order nonlinear Hall effect induced by the Berry-connection polarizability tensor, Nat. Nanotechnol. **16**, 869 (2021).
[55] H. Liu, J. Zhao, Y.-X. Huang, X. Feng, C. Xiao, W. Wu, S. Lai, W.-b. Gao, and S. A. Yang, Berry connection polarizability tensor and third-order Hall effect, Phys. Rev. B **105**, 045118 (2022).

[56] O. Pal and T. K. Ghosh, Polarization and third-order Hall effect in III-V semiconductor heterojunctions, Phys. Rev. B **109**, 035202 (2024).

[57] See Supplemental Material at http://link.aps.org/supplemental/10.1103/wb4y-tzln for additional figures showing BCP tensor components, field-induced Berry curvature, band structures, and Fermi surfaces for pure and hybrid altermagnetic orders.

[58] Datasets and codes are provided for figures shown in this paper at Zenodo, 2025, doi:10.5281/zenodo.17413838.